Gating Single-Molecule Fluorescence with Electrons

Katharina Kaiser, Song Jiang, Michelangelo Romeo, Fabrice Scheurer, Guillaume Schull, Anna Roslawska

Gating Single-Molecule Fluorescence with Electrons

Katharina Kaiser,[1,2,*] Song Jiang,[1] Michelangelo Romeo,[1] Fabrice Scheurer,[1] Guillaume Schull,[1,†] and Anna Rosławska[1,3,‡]

[1]Université de Strasbourg, CNRS, IPCMS, UMR 7504, F-67000 Strasbourg, France

[2]IV. Physical Institute—Solids and Nanostructures, Georg-August-Universität Göttingen, Göttingen, 37077, Germany

[3]Max Planck Institute for Solid State Research, Stuttgart 70569, Germany

(Received 18 March 2024; revised 4 July 2024; accepted 10 September 2024; published 8 October 2024)

Tip-enhanced photoluminescence (TEPL) measurements are performed with subnanometer spatial resolution on individual molecules decoupled from a metallic substrate by a thin NaCl layer. TEPL spectra reveal progressive fluorescence quenching with decreasing tip-molecule distance when electrons tunneling from the tip of a scanning tunneling microscope are injected at resonance with the molecular states. Rate equations based on a many-body model reveal that the luminescence quenching is due to a progressive population inversion between the ground neutral (S_0) and the ground charge (D_0^-) states of the molecule occurring when the current is raised. We demonstrate that the bias voltage and the lateral tip position can be used to gate the molecular emission. Our approach can be applied to any molecular system, providing unprecedented control over the fluorescence of a single molecule.

DOI: 10.1103/PhysRevLett.133.156902

Control over the optical properties of individual molecules can be achieved by modifying their chemical structure or influencing their local environment. In that respect, the ability to switch the molecule from a bright to a dark state is one of the most striking modifications of these characteristics. Such a mechanism is employed, for example, in superresolution microscopy to localize individual emitters [1–3] and holds the potential to be applied in sensors [4] or even molecular quantum devices [5] to gate the properties of single-photon emitters [6]. Usually, switching the chromophore to a dark state relies on a transition to a long-lived, nonemissive triplet state, or on modifying its redox state by attaching charges to prevent the formation of charge-neutral excited states [3,4,7,8]. The latter process can be induced by an electric stimulus, as in macroscopic electrochromic materials [7,9]. However, gating the photoluminescence of one targeted molecule by the controlled injection of single charges remains a thought experiment.

Scanning tunneling microscopy (STM) allows the controlled charge transfer to single molecules with sub-nm precision [10–16]. In addition, the field enhancement in the metallic tip-sample junction, acting as a plasmonic picocavity [17,18], enables probing electrically driven STM-induced luminescence (STML) [18–33] or optically driven tip-enhanced photoluminescence (TEPL) [34–38] of molecules with nearly atomic resolution. STML has been used in a few cases to address the fluorescence of charged species, however, the electrical excitation renders it impossible to disentangle luminescence and charge transport, i.e., to control them separately [25–33]. This issue can be circumvented using TEPL, however, so far the ability of the STM to control the transient charge state has not yet been exploited in this context.

Here, we show that we can manipulate the photoluminescence yield from a molecule located in the tunneling junction of an STM, up to nearly full luminescence quenching, by resonant charge transport through the molecule. We achieve this by adjusting the tip-molecule distance, the applied bias voltage, and the in-plane position of the tip with respect to the molecule. This versatile control of the fluorescence yield of a molecule with sub-nm precision is explained using a many-body description.

The experiments were performed with a low-temperature (6 K) ultrahigh vacuum STM equipped with two lenses used to focus the beam of a laser and collect the luminescence from the STM junction (see Supplemental Material [39]). The Ag(111) substrate was cleaned by argon-ion sputtering and annealing cycles. NaCl was thermally sublimed onto Ag(111) kept at room temperature and then mildly annealed to obtain two to four-monolayer NaCl films. The molecules were thermally sublimed onto the cold (6 K) NaCl/Ag(111) substrate. The electrochemically etched Ag STM tips

*Contact author: katharina.kaiser@uni-goettingen.de

†Contact author: guillaume.schull@ipcms.unistra.fr

‡Contact author: a.roslawska@fkf.mpg.de

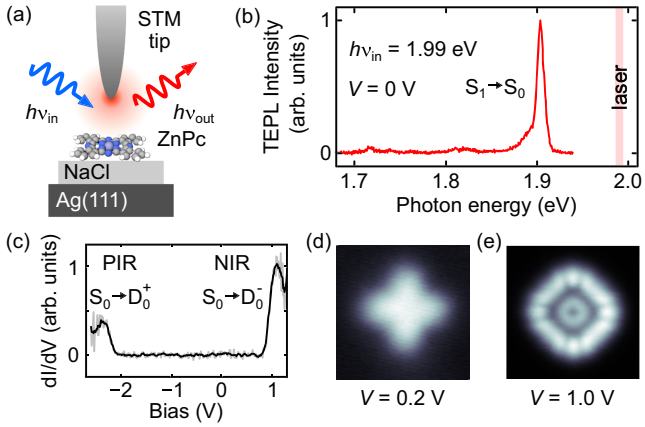

FIG. 1. (a) Experimental sketch. (b) TEPL spectrum of ZnPc. $h\nu_{in} = 1.99$ eV, laser power $P = 13$ μW, integration time $t = 10$ s, $V = 0$ V. (c) dI/dV spectrum of ZnPc. Set point: $V = 1.3$ V, $I = 20$ pA. (d) Constant-current STM image on 3 ML NaCl, $V = 0.2$ V, $I = 3$ pA. (e) Constant-height STM image, $V = 1$ V. Both images are 3×3 nm^2.

were sputtered and annealed in ultrahigh vacuum. The plasmonic response of the tips, which depends on their structure [18,34,40], was optimized by voltage pulses and gentle indentations into the Ag(111) substrate.

Figure 1(a) shows the experimental scheme. A zinc phthalocyanine (ZnPc) molecule deposited on 4 monolayer (ML) thick NaCl is optically excited by a tunable laser source focused on the tip-sample junction. The junction is acting as a plasmonic picocavity amplifying the electromagnetic field [18,34]. This leads to increased absorption and a strong enhancement of radiative transitions (Purcell effect) so that the TEPL signal of individual molecules can be detected in the far field [34–38]. A typical single-molecule TEPL spectrum (incident photon energy $h\nu_{in} = 1.99$ eV) is shown in Fig. 1(b). It reveals a prominent emission line at $h\nu_{out} = 1.91$ eV, and low-energy vibronic peaks. Both stem from the $S_1 \rightarrow S_0$ transition of neutral ZnPc [21,41]. Figure 1(c) shows a differential conductance (dI/dV) spectrum of ZnPc/4 ML NaCl/Ag(111) with two distinct features at $V = -2.1$ and $V = 0.8$ V, corresponding to the positive and negative ion resonances (PIR and NIR) [10]. For voltages between PIR and NIR (in-gap conditions), the charge transport through the junction is nonresonant and only perturbed by the presence of the molecule [42]. In contrast, at PIR and NIR, the charge transport is dominated by a two-step process where the molecule is first charged by tunneling from the tip and then discharged by tunneling to the sample. Thus, for resonant conditions, the molecule repetitively switches between neutral and charged. Figures 1(d) and 1(e) show STM images of ZnPc recorded in these two transport regimes, namely, in-gap ($V = 0.2$ V) and at NIR ($V = 1$ V); that is Fig. 1(e) shows the density of the lowest unoccupied molecular orbital (LUMO). All data in the main text are recorded for molecules on 4 ML NaCl, except for Fig. 1(d).

In the following, we investigate how charge transport influences the optical properties of the neutral molecule. Figure 2(a) shows a series of TEPL spectra recorded in gap ($V = 0.5$ V) for different tip-molecule distances Δz, defined relatively to an initial tip-molecule separation ($\Delta z = 0$) at a setpoint of $V = 1$ V and $I = 5$ pA. Upon approaching the tip to the molecule (decreasing Δz), the $S_1 \rightarrow S_0$ peak in TEPL increases in intensity, broadens from 6 meV to more than 10 meV (full width at half maximum), as extracted from Lorentzian fits, and shifts by 6 meV towards smaller energies at very small distances. This is in line with previous experiments [18], which assigned a similar behavior to an increased coupling between the molecular transition dipole moments and the plasmons upon reduction of the tip-molecule distance. The observed redshift can be attributed to a combination of Lamb and Stark effects. The same Δz dependence, but recorded at NIR ($V = 1$ V), is shown in Fig. 2(b). Up to $\Delta z \approx -150$ pm, the TEPL signal at resonance is similar to the one recorded in gap, i.e., it features similar intensity and peak broadening. For $\Delta z < -150$ pm, however, the photoluminescence intensity decreases and is almost entirely suppressed for $\Delta z \approx -400$ pm.

This gradual reduction of the emission yield with decreasing Δz, which is only observed at resonance, suggests a quenching mechanism related to the transient charging of the molecule. To confirm this, we recorded the tunnel current simultaneously with the integrated TEPL intensity of the $S_1 \rightarrow S_0$ transition [Figs. 2(c) and 2(d)]. Note that, for $V = 0.5$ V and $\Delta z > -250$ pm, the current is too low to be measured. At $\Delta z > -150$ pm, where $I(\Delta z)$ recorded at resonance follows the expected exponential dependence [red squares in Fig. 2(d)], the TEPL intensity increases similarly for both bias voltages. Upon approaching the molecule ($\Delta z < -150$ pm), $I(\Delta z)$ measured at resonance deviates from the exponential dependence, while the TEPL intensity slowly decreases. This behavior contrasts with the TEPL intensity recorded in-gap that increases monotonically with the tip approach [gray scale circles in Fig. 2(c)]. Eventually, at very small distances and for resonant tunneling conditions [blue squares in Figs. 2(c) and 2(d)], the current saturates ($I_{sat} \approx 400$ pA), and the TEPL intensity is nearly fully quenched.

The saturation in the tunnel current is a direct consequence of the charge transport mechanism that takes place in the double-barrier tunneling junction [16,43]. At NIR, the molecule is successively charged negatively by an electron tunneling through the vacuum barrier from the tip to the molecule, and then discharged by a second tunneling event through NaCl. The net tunnel current is limited by the process with the lower tunneling probability (*i.e.*, the slower process). While the tunneling probability through the vacuum gap varies with Δz, the one through NaCl is merely determined by the thickness of NaCl and thus remains constant as the tip approaches. At large

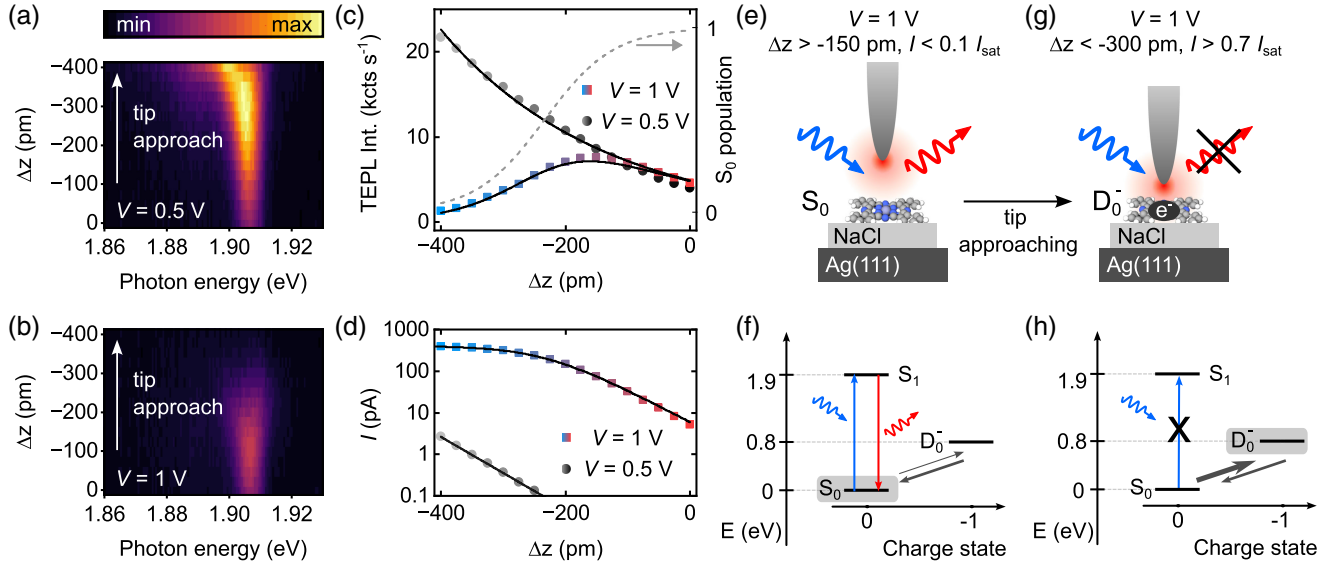

FIG. 2. (a),(b) TEPL spectra as a function of Δz for $V = 0.5$ (a) and $V = 1$ V (b). The bottom spectra are recorded at $\Delta z = 0$, then the tip is approached in 25 pm intervals. $h\nu_{\text{in}} = 1.99$ eV, $P = 3$ μW, $t = 4$ s. The color scale is the same for both panels. (c) Integrated TEPL intensity (1.88 eV $< h\nu_{\text{out}} <$ 1.92 eV) for $V = 0.5$ V [gray scale circles, panel (a)] and $V = 1$ V [red-blue squares, panel (b)] as a function of Δz. The black and red shadings indicate the Δz range in which the tunnel current increases exponentially, light gray and blue shadings indicate the saturation regime. The solid lines are fits to the model discussed in the main text, the dashed gray line shows the relative population of the ground S_0 state. (d) Tunneling current recorded together with measurements in (c), the solid line for $V = 1$ V is a fit to Eq. (1), and the solid line for $V = 0.5$ V is an exponential fit. (e)–(h) Sketches of the experimental conditions (e),(g) and many-body diagrams for large (f) and small (h) tip-sample distances. The gray boxes in (f),(h) indicate the state that is populated most of the time.

tip-molecule distances, tunneling through the vacuum is, therefore, the rate-limiting process [$\Delta z > -150$ pm, Figs. 2(e) and 2(f)], and the tunneling current increases exponentially with decreasing Δz. At smaller tip-molecule distances ($\Delta z < -150$ pm) the progressive saturation of the current indicates that the discharging process through NaCl becomes the rate-limiting step. This affects the relative populations of the neutral S_0 and charged D_0^- states of the molecule [Figs. 2(f) and 2(h)]: At large distances ($\Delta z > -150$ pm), the charging rate (indicated by the dark gray arrow) is low and the molecule spends most of the time in the neutral S_0 state. Optical excitation of the $S_0 \rightarrow S_1$ transition and the emission from the reverse $S_1 \rightarrow S_0$ transition [Fig. 2(f)] are thus possible. For decreasing Δz, the population of the negatively charged D_0^- state increases at the expense of the S_0 population, up to a predominant occupation of D_0^- in the saturation regime [Figs. 2(g) and 2(h)]. Since the $D_0^- \rightarrow S_1$ transition cannot be induced by a photon, the formation of a neutral exciton is gradually hindered and the TEPL signal vanishes. Thus, the transition to a configuration where the charged doublet state is occupied most of the time is responsible for the quenching of the luminescence, akin to the process taking place in electrochromic systems. A similar effect is expected to take place at PIR when the D_0^+ population is promoted. At this condition, however, electrical excitation of S_1 via D_0^+ leads to a strong STML signal at the same photon energy [27,31,33,44], precluding the observation of the photoluminescence quenching (see Supplemental Material [39]).

To quantify the mechanism behind the photoluminescence quenching, we develop a model encompassing the many-body transitions between the relevant states in our system, S_0, S_1, and D_0^-, illustrated in Figs. 2(f) and 2(h) (see also Supplemental Material [39]). The total tunnel current through the double-barrier tunneling junction can be expressed using the tunneling rates through vacuum, $\Gamma_{\text{vac}}(\Delta z)$ ($S_0 \rightarrow D_0^-$ transition), and NaCl, Γ_d ($D_0^- \rightarrow S_0$ transition), respectively [16]:

$$I(\Delta z) = \frac{q\Gamma_{\text{vac}}^0}{\exp(2\kappa_{\text{vac}}\Delta z) + \Gamma_{\text{vac}}^0 \tau_d}, \tag{1}$$

with the elementary charge q, the tunneling rate from the tip Γ_{vac}^0 for $\Delta z = 0$, the decay constant κ_{vac} and the D_0^- lifetime $\tau_d = \Gamma_d^{-1}$. The steady-state ground state population N_{S_0} is

$$N_{S_0} = \frac{1}{1 + \tau_d \Gamma_{\text{vac}}^0 \exp(-2\kappa_{\text{vac}}\Delta z)}. \tag{2}$$

Fitting $I(\Delta z)$ recorded for $V = 1$ V in Fig. 2(d) (solid line) with Eq. (1) yields $\tau_d \approx 400$ ps, in line with recent reports [16,45]. Once the tunneling rate from the tip becomes comparable to the tunneling rate from the

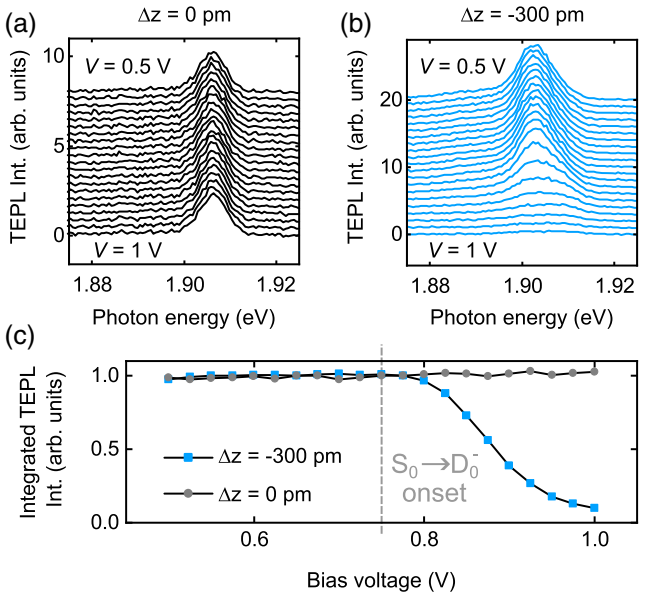

FIG. 3. (a),(b) TEPL spectra as a function of bias voltage for two different Δz (voltage steps of 25 mV). $h\nu_{\mathrm{in}} = 1.99$ eV, $P = 3$ μW, $t = 5$ s. (c) Integrated and normalized TEPL intensity from panels (a) and (b), integration range: 1.88 eV < $h\nu_{\mathrm{out}}$ < 1.92 eV.

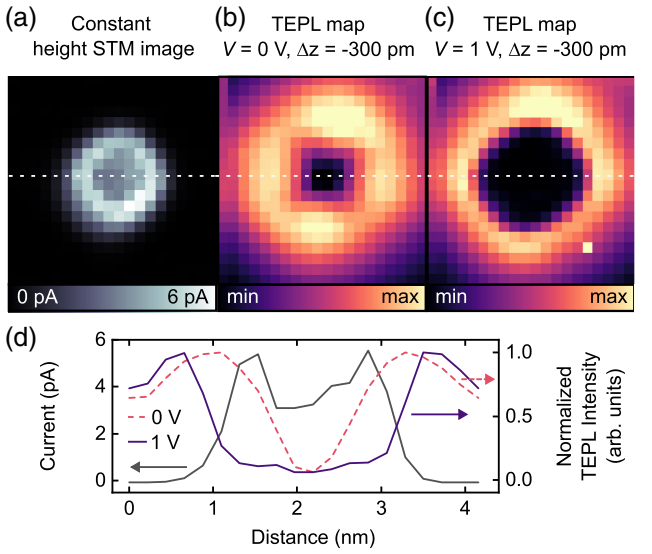

FIG. 4. (a) Constant height STM image of ZnPc, $V = 1$ V. (b),(c) Constant height TEPL maps on the same molecule as in a); $h\nu_{\mathrm{in}} = 1.99$ eV, $P = 3$ μW, integration time $t = 2$ s per pixel. Integration range: 1.88 eV < $h\nu_{\mathrm{out}}$ < 1.92 eV. All images are 4.4×4.4 nm^2. (d) Cross section along the dashed lines in (a)–(c). Current is plotted on the left axis and normalized TEPL intensity on the right axis.

substrate (here for $\Delta z < -150$ pm), N_{S_0} begins to substantially deviate from 1 [dashed line in Fig. 2(c)].

Next, we analyze the $S_0 \rightarrow S_1$ and $S_1 \rightarrow S_0$ transitions that are responsible for the observed photoluminescence. The total light intensity can be written as $P(\Delta z) = \Gamma_{\mathrm{ex}} N_{S_0}$, where Γ_{ex} is the excitation rate. In agreement with recent literature [34,36], we find that $\Gamma_{\mathrm{ex}}(\Delta z)$ is well described by an exponential function, reflecting the strongly increased plasmonic field when the tip approaches the molecule. Therefore,

$$P(\Delta z) = \Gamma_{\mathrm{ex}}^{0} \exp(-\alpha \Delta z) N_{S_0} \tag{3}$$

with Γ_{ex}^{0} being the excitation rate for $\Delta z = 0$ and α the decay constant. Fitting the data in Fig. 2(c) with Eq. (3) and $N_{S_0} = 1$ for $V = 0.5$ V, that is assuming very short excited state lifetime [18,38] and thus $N_{S_1} \approx 0$, we obtain a very good agreement with the experiment. For fitting the curve recorded at $V = 1$ V, we use the same values of Γ_{ex}^{0} and α, but N_{S_0} described by Eq. (2). Again, there is excellent agreement with the experiment. Comparing $P(\Delta z, V = 1\ \mathrm{V})$ and $N_{S_0}(\Delta z)$ in Fig. 2(c), we find that the quenching sets in already for $N_{S_0} \approx 0.8$, at $\Delta z = -150$ pm.

Since the ability to excite a molecule with photons depends on the relative population of S_0, we can gate TEPL by the applied bias voltage. Figures 3(a) and 3(b) show constant-height TEPL spectra as a function of the applied bias voltage for large ($\Delta z = 0$ pm) and small ($\Delta z = -300$ pm) tip-molecule distances. At $\Delta z = 0$ pm [Fig. 3(a)], TEPL remains unaffected by the change in bias voltage from 0.5 V to 1 V. In contrast, at small distances [Fig. 3(b)], increasing the bias from 0.5 to 1 V results in quenching. The integrated TEPL intensity as a function of bias voltage for these two distances is compared in Fig. 3(c) At large tip-molecule distances (gray circles), the TEPL signal intensity remains constant. For small distances (blue squares), it begins decreasing at $V > 0.75$ V, a value that matches the onset of the NIR [Fig. 1(d)]. At large distances, the tunneling probability between the tip and molecule is low, and thus the relative population of S_0 remains high regardless of the bias voltage. This is also true at small distances for low bias voltages, as D_0^- cannot be accessed. Hence, in both conditions, the TEPL signal remains intense. In contrast, at small distances and at bias voltages resonant with the NIR, D_0^- is efficiently populated and the luminescence is quenched.

The local character of this gating is demonstrated by the TEPL intensity dependence on the tip position. Figure 4(a) shows the spatial extent of the LUMO ($V = 1$ V). Figures 4(b) and 4(c) show maps of the TEPL intensity recorded atop the molecule in-gap (b) and at NIR (c) for $\Delta z = -300$ pm. The map recorded at $V = 0$ V reveals a radially symmetrical pattern and a low intensity region in the middle of the molecule. This expected spatial dependence originates from the coupling of the picocavity plasmon to the doubly degenerate transition dipoles of S_1 for ZnPc. The low intensity in the center arises due to the symmetry of the system which leads to a vanishing coupling between the picocavity field

and the molecular transition density [34,46]. At resonant tunneling conditions [$V = 1$ V, Fig. 4(c)], the TEPL map reveals a much broader dark center compared to the one at $V = 0$ V. This dark region matches well the spatial extent of the LUMO in the current map in Fig. 4(a). In contrast, in regions where resonant tunneling through the molecule is not possible (at tip positions exceeding the lateral extent of the LUMO) the intensity pattern of Fig. 4(b) is recovered. This demonstrates that, for $V = 1$ V and $\Delta z = -300$ pm, as soon as direct tunneling into the ZnPc is possible, we can quench TEPL by controllably decreasing the population of S_0. This is further illustrated in the cross section in Fig. 4(d), where the onset of the orbital coincides with the onset of TEPL quenching. The S_0 occupancy in the current saturation regime [Fig. 2(d)] is entirely governed by the substrate-mediated discharging rate and is therefore independent of the tip position. Overall, this photoluminescence quenching strategy can be generalized to other molecules and different NaCl thicknesses as we demonstrate in the Supplemental Material for H_2Pc on 3 ML NaCl [39].

In conclusion, we used the tip of an STM simultaneously as an atomically precise electrode, which allowed us to modify the charge state of a molecule, and as an optical antenna to probe its photoluminescence. By selectively injecting charges into the molecule we can controllably shift the population of the molecule from its neutral S_0 ground state to a transient charge state D_0^- from which the neutral exciton cannot be formed. Our approach can be used, for example, to selectively alter the properties of individual chromophores in a molecular layer or assembly. This can influence coherent dipole-dipole coupling [21–23] or energy transfer mechanisms [20,24], thus modifying the collective optical responses of the system.

Acknowledgments—We thank Tomáš Neuman, Klaus Kuhnke, and Stéphane Berciaud for fruitful discussions and Virginie Speisser and Halit Sumar for technical support. This project has received funding from the European Research Council (ERC) under the European Union's Horizon 2020 research and innovation program (Grant Agreement No. 771850). This work of the Interdisciplinary Thematic Institute QMat, as part of the ITI 2021 2028 program of the University of Strasbourg, CNRS and Inserm, was supported by IdEx Unistra (ANR 10 IDEX 0002), and by Structure de la formation par la recherche dans les initiatives d'excellence STRAT'US Project No. (ANR 20 SFRI 0012) and Ecole Universitaire de Recherche en Sciences quantiques et nanomatériaux ANR-17-EURE-0024 under the framework of the French Investments for the Future Program. K. K. acknowledges funding from the SNSF under the Postdoc.Mobility Grant Agreement No. 206912. A. R. acknowledges funding from the Emmy Noether Programme of the Deutsche Forschungsgemeinschaft (DFG, German Research Foundation)—534367924.

[1] J. Fölling *et al.*, Fluorescence nanoscopy by ground-state depletion and single-molecule return, Nat. Methods **5**, 943 (2008).
[2] M. Heilemann, S. van de Linde, A. Mukherjee, and M. Sauer, Super-resolution imaging with small organic fluorophores, Angew. Chem., Int. Ed. **48**, 6903 (2009).
[3] J. Vogelsang, T. Cordes, C. Forthmann, C. Steinhauer, and P. Tinnefeld, Controlling the fluorescence of ordinary oxazine dyes for single-molecule switching and superresolution microscopy, Proc. Natl. Acad. Sci. U.S.A. **106**, 8107 (2009).
[4] S. Brasselet and W. Moerner, Fluorescence behavior of single-molecule pH-sensors, Single Mol. **1**, 17 (2000).
[5] C. Toninelli *et al.*, Single organic molecules for photonic quantum technologies, Nat. Mater. **20**, 1615 (2021).
[6] M. Yu, D. Yim, H. Seo, and J. Lee, Electrical charge control of h-BN single photon sources, 2D Mater. **9**, 035020 (2022).
[7] Z. Ji, S. K. Doorn, and M. Sykora, Electrochromic graphene molecules, ACS Nano **9**, 4043 (2015).
[8] R. M. Dickson, A. B. Cubitt, R. Y. Tsien, and W. E. Moerner, On/off blinking and switching behaviour of single molecules of green fluorescent protein, Nature (London) **388**, 355 (1997).
[9] C. Gu, A.-B. Jia, Y.-M. Zhang, and S. X.-A. Zhang, Emerging electrochromic materials and devices for future displays, Chem. Rev. **122**, 14679 (2022).
[10] J. Repp, G. Meyer, S. M. Stojković, A. Gourdon, and C. Joachim, Molecules on insulating films: Scanning-tunneling microscopy imaging of individual molecular orbitals, Phys. Rev. Lett. **94**, 026803 (2005).
[11] G. V. Nazin, S. W. Wu, and W. Ho, Tunneling rates in electron transport through double-barrier molecular junctions in a scanning tunneling microscope, Proc. Natl. Acad. Sci. U.S.A. **102**, 8832 (2005).
[12] I. Swart, T. Sonnleitner, and J. Repp, Charge state control of molecules reveals modification of the tunneling barrier with intramolecular contrast, Nano Lett. **11**, 1580 (2011).
[13] I. Fernández-Torrente, D. Kreikemeyer-Lorenzo, A. Stróżecka, K. J. Franke, and J. I. Pascual, Gating the charge state of single molecules by local electric fields, Phys. Rev. Lett. **108**, 036801 (2012).
[14] N. Hauptmann, C. Hamann, H. Tang, and R. Berndt, Switching and charging of a ruthenium dye on Ag(111), Phys. Chem. Chem. Phys. **15**, 10326 (2013).
[15] K. A. Cochrane *et al.*, Molecularly resolved electronic landscapes of differing acceptor-donor interface geometries, J. Phys. Chem. C **122**, 8437 (2018).
[16] K. Kaiser, L.-A. Lieske, J. Repp, and L. Gross, Charge-state lifetimes of single molecules on few monolayers of NaCl, Nat. Commun. **14**, 4988 (2023).
[17] F. Benz *et al.*, Single-molecule optomechanics in "picocavities," Science **354**, 726 (2016).
[18] A. Rosławska, T. Neuman, B. Doppagne, A. G. Borisov, M. Romeo, F. Scheurer, J. Aizpurua, and G. Schull, Mapping Lamb, Stark, and Purcell effects at a chromophore-picocavity junction with hyper-resolved fluorescence microscopy, Phys. Rev. X **12**, 011012 (2022).
[19] X. H. Qiu, G. V. Nazin, and W. Ho, Vibrationally resolved fluorescence excited with submolecular precision, Science **299**, 542 (2003).

[20] H. Imada *et al.*, Real-space investigation of energy transfer in heterogeneous molecular dimers, Nature (London) **538**, 364 (2016).
[21] Y. Zhang *et al.*, Visualizing coherent intermolecular dipole–dipole coupling in real space, Nature (London) **531**, 623 (2016).
[22] B. Doppagne, M. C. Chong, E. Lorchat, S. Berciaud, M. Romeo, H. Bulou, A. Boeglin, F. Scheurer, and G. Schull, Vibronic spectroscopy with submolecular resolution from STM-induced electroluminescence, Phys. Rev. Lett. **118**, 127401 (2017).
[23] Y. Luo *et al.*, Electrically driven single-photon superradiance from molecular chains in a plasmonic nanocavity, Phys. Rev. Lett. **122**, 233901 (2019).
[24] S. Cao *et al.*, Energy funnelling within multichromophore architectures monitored with subnanometre resolution, Nat. Chem. **13**, 766 (2021).
[25] B. Doppagne *et al.*, Electrofluorochromism at the single-molecule level, Science **361**, 251 (2018).
[26] V. Rai *et al.*, Boosting light emission from single hydrogen phthalocyanine molecules by charging, Nano Lett. **20**, 7600 (2020).
[27] J. Doležal, S. Canola, P. Merino, and M. Švec, Exciton-trion conversion dynamics in a single molecule, ACS Nano **15**, 7694 (2021).
[28] J. Doležal *et al.*, Real space visualization of entangled excitonic states in charged molecular assemblies, ACS Nano **16**, 1082 (2021).
[29] J. Doležal *et al.*, Evidence of exciton-libron coupling in chirally adsorbed single molecules, Nat. Commun. **13**, 6008 (2022).
[30] S. Jiang, T. Neuman, R. Bretel, A. Boeglin, F. Scheurer, E. Le Moal, and G. Schull, Many-body description of STM-induced fluorescence of charged molecules, Phys. Rev. Lett. **130**, 126202 (2023).
[31] T.-C. Hung, R. Robles, B. Kiraly, J. H. Strik, B. A. Rutten, A. A. Khajetoorians, N. Lorente, and D. Wegner, Bipolar single-molecule electroluminescence and electrofluorochromism, Phys. Rev. Res. **5**, 033027 (2023).
[32] V. Rai *et al.*, Activating electroluminescence of charged naphthalene diimide complexes directly adsorbed on a metal substrate, Phys. Rev. Lett. **130**, 036201 (2023).
[33] K. Kaiser *et al.*, Electrically driven cascaded photon-emission in a single molecule, arXiv:2402.17536.
[34] B. Yang *et al.*, Sub-nanometre resolution in single-molecule photoluminescence imaging, Nat. Photonics **14**, 693 (2020).
[35] H. Imada *et al.*, Single-molecule laser nanospectroscopy with micro–electron volt energy resolution, Science **373**, 95 (2021).
[36] M. Imai-Imada *et al.*, Orbital-resolved visualization of single-molecule photocurrent channels, Nature (London) **603**, 829 (2022).
[37] A. Rosławska *et al.*, Submolecular-scale control of phototautomerization, Nat. Nanotechnol. **19**, 738 (2024).
[38] J. Doležal, A. Sagwal, R. C. de Campos Ferreira, and M. Švec, Single-molecule time-resolved spectroscopy in a tunable STM nanocavity, Nano Lett. **24**, 1629 (2024).
[39] See Supplemental Material at http://link.aps.org/supplemental/10.1103/PhysRevLett.133.156902 for additional methods, experimental data, and details on the model.
[40] J. Aizpurua, S. P. Apell, and R. Berndt, Role of tip shape in light emission from the scanning tunneling microscope, Phys. Rev. B **62**, 2065 (2000).
[41] C. Murray *et al.*, Visible luminescence spectroscopy of free-base and zinc phthalocyanines isolated in cryogenic matrices, Phys. Chem. Chem. Phys. **13**, 17543 (2011).
[42] A. Grewal, C. C. Leon, K. Kuhnke, K. Kern, and O. Gunnarsson, Character of electronic states in the transport gap of molecules on surfaces, ACS Nano **17**, 13176 (2023).
[43] W. Steurer, L. Gross, and G. Meyer, Local thickness determination of thin insulator films via localized states, Appl. Phys. Lett. **104**, 231606 (2014).
[44] J. Doležal *et al.*, Charge carrier injection electroluminescence with CO-functionalized tips on single molecular emitters, Nano Lett. **19**, 8605 (2019).
[45] A. Rosławska *et al.*, Single charge and exciton dynamics probed by molecular-scale-induced electroluminescence, Nano Lett. **18**, 4001 (2018).
[46] T. Neuman, R. Esteban, D. Casanova, F. J. García-Vidal, and J. Aizpurua, Coupling of molecular emitters and plasmonic cavities beyond the point-dipole approximation, Nano Lett. **18**, 2358 (2018).